IEEE Access
Multidisciplinary | Rapid Review | Open Access Journal

Received September 27, 2020, accepted October 27, 2020, date of publication November 6, 2020,
date of current version November 19, 2020.

Digital Object Identifier 10.1109/ACCESS.2020.3036384

Optimal Power Allocation Algorithm for Multi-Mode OFDM-OAM Communication Systems in Multipath Channel

MINGZHE QU[1], YANG WANG[2], (Member, IEEE), XI LIAO[2,3], (Member, IEEE), SHASHA LIAO[2], AND JIHUA ZHOU[3]

[1]School of Technology, Harbin University, Harbin 150001, China
[2]Chongqing Key Laboratory of Mobile Communications Technology, Engineering Research Center of Mobile Communications of the Ministry of Education, School of Communication and Information Engineering, Chongqing University of Posts and Telecommunications, Chongqing 400065, China
[3]Chongqing Jinmei Communication Company Ltd., Chongqing 400065, China

Corresponding authors: Mingzhe Qu (qmz7652@163.com) and Yang Wang (wangyang@cqupt.edu.cn)

This work was supported in part by the National Natural Science Foundation of China under Grant 61801062 and Grant 61801063; in part by the State Key Laboratory of Millimeter Waves under Grant K202032; in part by the China Postdoctoral Science Foundation under Grant 2019M653826XB; and in part by the Chongqing Research Program of Basic Research and Frontier Technology under Grant CSTC2017JCYJA0817.

ABSTRACT Vortex wave carrying orbital angular momentum (OAM), an important property of electromagnetic wave, has bridged a new way to achieve high-capacity radio-frequency communications using different OAM-modes. However, the system performance of OAM multiplexing with orthogonal-frequency-division multiplexing (OFDM) technologies has not been thoroughly investigated in multipath channel environment. In this paper, we first built up the uniform circular array (UCA)-based multi-mode OFDM-OAM communication system, where the reflected paths has been generated based on ideal specular reflector. Based on the multi-mode OFDM-OAM communication system model, we also derived the two-path OAM channel model with the direct and reflected paths. Then, we proposed a robust optimal power allocation algorithm by decomposing the whole optimization problem into inner-layer OAM-modes optimization and outer-layer OFDM subcarriers optimization in order to control the allocated power flexibly based on the channel quality differences between OAM-modes. The simulation results demonstrate that the proposed algorithm can significantly increase the channel capacity for multi-mode OFDM-OAM communications in multipath channel as compared with the traditional equal power allocation method and has a considerable low computational complexity than the binary search water-filling method when the number of OFDM subcarriers is large enough.

INDEX TERMS Orbital angular momentum (OAM), orthogonal frequency-division multiplexing-orbital angular momentum (OFDM-OAM), power allocation, spectrum efficiency, multipath transmission channel.

I. INTRODUCTION

A recent discovery of electromagnetic waves enables the ability to multiplex multiple beams carrying orbital angular momentum (OAM), OAM waves have the helical phase front described by a phase factor of $\exp(jl\varphi)$, where φ is the transverse azimuth angle, l is an arbitrary integer representing OAM mode number [1]–[3]. Although OAM has an infinite-dimensional orthogonal basis theoretically, only a set of mutually orthogonal OAM-modes can be utilized to perform the multiplexing and demultiplexing for several coaxial parallel data streams transmission efficiently in practice. Thereby, OAM as a novel resources can potentially achieve high spectral efficiencies at the same frequency channel for communication applications including free space optics, optical fiber installation, underwater wireless, wireless indoor connections, and wireless communications [4]–[9].

Vortex electromagnetic (EM) waves carrying OAM exerts a tremendous fascination on researchers as a promising Beyond fifth generation (B5G) technique in recent years and a significant research effort has mainly been concentrated

The associate editor coordinating the review of this manuscript and approving it for publication was Urbashi Mitra.

on how to achieve high spectrum efficiency in wireless communications. The OAM-based multiple-input multiple-output (MIMO) multiplexing system has been demonstrated to obtain high capacity gains while communication distance is not long enough [10], [11]. The combination of OAM with traditional MIMO, and even massive MIMO is a design that is expected to reach the goal of the maximum capacity. Recently, an ocean of effort has been spent on researching key solutions, such as OAM-MIMO multiplexing transmission, beam steering for the misalignment cases, OAM waves generation, and so on [12]–[15].

However, most existing researches mainly pour attention into the line-of-sight (LoS) wireless communications. Unfortunately, multipath effects, caused by beam spreading and reflection and refraction from the surrounding objects, are inevitable and are likely to have significant effects on the performance of OAM multiplexing systems [16], [17]. The multipath effects of millimeter wave communication link using OAM multiplexing at 28 GHz have been investigated in [16]. Results have demonstrated that the multipath caused by specular reflection from an ideal parallel reflector induces intra- and inter-channel crosstalk. Fortunately, we have noticed that the anti-multipath property of orthogonal frequency division multiplexing (OFDM) technique can be utilized to mitigate the inter-symbol interference or the channel crosstalk for broadband wireless communications. The compatibility between OAM and the traditional OFDM has been proven, which can achieve extremely high capacity in OAM communications [18]–[21]. The experimental investigation has been presented to indicate the inter-symbol interference caused by multipath effects for OAM channel using OFDM, and the results have demonstrated that an channel with high order OAM-modes tends to suffer from stronger intra- and inter-channel crosstalk [18]. The transceiver architecture based on a flexible two-dimensional fast Fourier transform algorithm for OAM-OFDM communication is investigated in [19], which considers a typical two-path scenario. Considering the overhead in hardware and the computational complexity in software, the researchers of [20] proposed a time-switched OFDM-OAM MIMO system by performing a time-switched sequence in the baseband, and analyzed spectrum efficiency for LoS OAM wireless transmissions. The authors have proposed the joint OAM multiplexing and the traditional OFDM scheme in sparse multipath environments, and demonstrated that the phase difference compensation can drastically increase channel capacity [21].

On the other hand, the maximum system capacity can be obtained by performing optimal power allocation algorithms under the condition of total power limitation and perfect channel state information (CSI). The water-filling algorithm is a typical optimal power allocation algorithm, which mainly includes the binary search water-filling algorithm [22], the iterative water-filling algorithm [23] and the linear water-filling algorithm [24]. An optimal power allocation algorithm is proposed to obtain maximum average spectrum efficiency of OFDM-OAM systems using the water-filling algorithm in [25], in which the channel quality differences between OAM channels with different modes are not considered. Notably, for OFDM-OAM communication in multipath channels, the number of subchannels is raised from the number of OAM-modes L to the product of the number of subcarriers S and the number of OAM-modes L. If the total power is allocated to all subchannels directly, it will not only lead to a decrease in flexibility which is formidable to control the power of single OAM-mode, but the trigger excessive complexity when the number of OFDM subcarriers is large enough. In fact the vortex waves carrying different OAM-modes are independent in multi-mode OFDM-OAM communications, it is not suitable to adopt the traditional water-filling algorithm directly. Thereby, it is paramount to propose an optimal power allocation algorithm for OFDM-OAM communications under multipath propagation condition.

In this paper we propose an optimal power allocation algorithm based on OAM-modes selection and binary search water-filling algorithm in typical two-path scenario for near-field OFDM-OAM communication. Also we present how to allocate the total power in order to control the transmitted power for all OAM modes flexibility and ensure the maximum capacity with relatively low complexity.

The rest of this paper is organized as follows. Section II presents the multi-mode OFDM-OAM system and deduces theoretically channel model in two-path scenario. Section III proposes an optimal power allocation algorithm with low complexity by jointly considering OAM modes and subcarriers constraints. Section IV evaluate the proposed algorithm for OFDM-OAM communication system. Conclusions are drawn in Section V.

II. SYSTEM MODEL

In this section, we give the multi-mode OFDM-OAM wireless communication system model in Fig. 1 based on a parallel ideal reflector. The system consists of S-point inverse discrete Fourier transform (IDFT) operator in the frequency domain, OAM-modes modulation, and transmit UCA at the transmitter as well as receive UCA, OAM-modes demodulation, and S-point discrete Fourier transform (DFT) operator at receiver. A reflector with a reflection coefficient of 100% is placed at a distance of h away from the center of transmitting UCA.

The multi-mode OAM beams are generated by propagating a set of orthogonal OAM-modes through transmit UCA equipped with N antenna elements. A part of multi-mode OAM beams will be reflected due to beam divergence. Since the reflection only change the sign of OAM mode, the reflected beams can be observed as an off-axis OAM beam with opposite mode from an imaging transmit UCA. Another UCA with M antenna elements can be used to receive the superposition of the direct OAM beam from the original link and the reflected OAM beam from an off-axis link, which is placed at a distance of $2h$ away from the center of the transmit UCA. The multiple OAM-modes multiplexing transmission

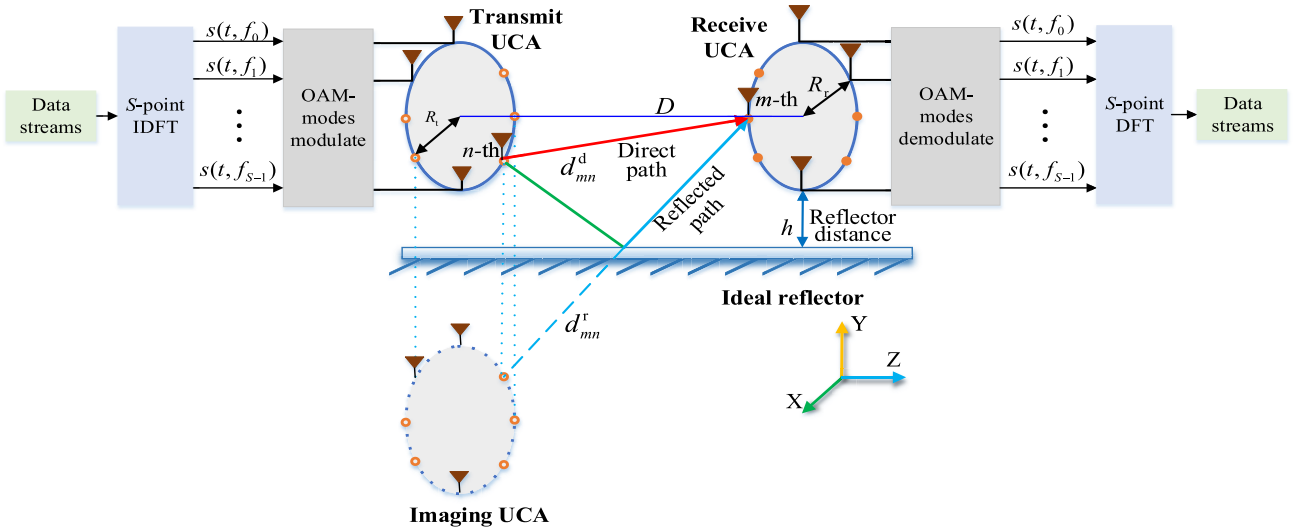

FIGURE 1. System model of the multi-mode OFDM-OAM communications with direct and reflected paths.

and demultiplexing receiving are both simply realized by a phase-shifter networking (PSN) which can generate a control signal with the same amplitude but different phase. The received OAM beams, consisting of an OAM beam with an OAM mode of l as well as a reflected beam with an OAM mode of -l, can be converted back to be a beam with $l = 0$ for detection at receiver end. Because the reflected OAM beams are along the off-axis, the orthogonality is no longer to the OAM beam in the direct path, so that reflection is likely to distort the spiral wavefront phase and cause the distortion of the OAM beam intensity. For simplicity, we assume that the UCA of the transmitter and receiver are perfectly aligned along a common central axis to ensure high efficiency and stability of OFDM-OAM communications in this paper.

At the transmitter, the transmitted OFDM signals, denoted by $s(t, f_s)$, can be obtained by modulating the original information symbol $s(t)$ with the s-th subcarrier frequency, and is given by

$$s(t, f_s) = s(t)e^{j2\pi f_s t} \tag{1}$$

The OAM signals with different modes can be generated by continuously feeding each antenna element of the transmit UCA. For the s-th subcarrier block, the OFDM-OAM radio vortex signal with mode l and frequency f_s, denoted by $x_{s,n,l}(t)$, on the n-th transmit array-element is given by

$$x_{s,n,l}(t) = \frac{p_{l,s}}{\sqrt{NS}} s_{l,s} e^{j2\pi f_s t} e^{jl\varphi_n} \tag{2}$$

where f_s is the s-th ($s = 0, 1, \ldots, S-1$) subcarrier frequency and subcarriers set is denoted as $=\{f_0, f_1 \ldots, f_{S-1}\}$, $s_{l,s}$ is the transmit modulated signal with an OAM mode of l corresponding to subcarrier frequency f_s, $p_{l,s}$ denotes the allocated power of the information symbol $s_{l,s}$, and $\varphi_n = 2\pi(n-1)/N$ is the azimuth angle for the n-th transmit array-element. Clearly, we can consider that the emitted OFDM symbol block is sampled by performing an N-point inverse discrete Fourier transform (IDFT) in spatial domain.

The transmit UCA can generate multiple OFDM-OAM signals with different OAM modes and subcarriers simultaneously; therefore, the total excitation on the n-th array-element is the linear superposition of each independent OFDM-OAM vortex signal. Thus, the corresponding s-th subcarrier vortex signal, denoted by $x^{d}_{s,n}(t)$, of the direct path for the n-th element can be expressed as

$$\begin{aligned} x^{d}_{s,n}(t) &= \sum_{l\in\mathcal{L}} x_{s,n,l}(t) \\ &= \sum_{l\in\mathcal{L}} \frac{p_{l,s}}{\sqrt{N}} s_{l,s} e^{j2\pi f_s t} e^{j\frac{2\pi n}{N} l} \end{aligned} \tag{3}$$

where $\mathcal{L} = \{\lfloor -N/2 + 1 \rfloor, \cdots, 0, 1, \cdots \lfloor N//2 \rfloor$ denotes the index set of OAM-modes.

Based on specular reflection model [14], reflection only changes the sign of OAM modes, so that the vortex signal generated by the imaging transmitting UCA, of the reflection paths for the s-th subcarrier block is

$$\begin{aligned} x^{r}_{s,n}(t) &= \sum_{l\in\mathcal{L}} x_{s,n,-l}(t) \\ &= \sum_{l\in\mathcal{L}} \frac{p_{l,s}}{\sqrt{N}} s_{l,s} e^{j2\pi f_s t} e^{-j\frac{2\pi n}{N} l} \end{aligned} \tag{4}$$

The response function $h_{mn}(t)$ of the channel matrix $\mathbf{H}$ can be expressed as $h_{mn}(t) = h(d_{mn})\delta(t)$ by the propagation distance d_{mn}. The expression of channel amplitude gain for the s-th subcarrier, denoted by $h_s(d_{mn})$, between the n-th transmitting antenna and the m-th receiving antenna is $h_s(d_{mn}) = \eta_s/d_{mn} \cdot \exp(-jk_s d_{mn})$, where $\eta_s = \beta\lambda_s/4\pi$ is a constant corresponding to the attenuation in which λ_s is the s-th carrier wavelength, $k_s = 2\pi/\lambda_s$ denotes the wavenumber, and $\delta(t)$ denotes the impulse response function with respect to t. According to the geometric relationship

shown in Fig. 1, we can derive the corresponding transmission distances, denoted by d_{mn}^{d} for direct link and d_{mn}^{r} for reflection link, from the n-th ($0 \le n \le N-1$) transmitting element to the m-th ($0 \le m \le M-1$) receiving element as,

$$d_{mn}^{\mathrm{d}} = [D^2 + R_t^2 + R_r^2 - 2R_{\mathrm{t}}R_{\mathrm{r}}\cos(\theta_m - \varphi_n)]^{1/2} \quad (5)$$

and

$$d_{mn}^{\mathrm{r}} = [D^2 + R_{\mathrm{t}}^2 + R_{\mathrm{r}}^2 - 2R_{\mathrm{t}}R_{\mathrm{r}}\cos(\theta_m - \varphi_n) + 4h\,(h - R_{\mathrm{t}}\sin\varphi_n - R_{\mathrm{r}}\sin\theta_m)]^{1/2} \quad (6)$$

respectively, where D is the transmission distance from the transmit UCAs center to the receive UCAs center, $\theta_m = \left[\frac{2\pi(m-1)}{M} + \theta_0\right]$ and $\varphi_n = \left[\frac{2\pi(n-1)}{N} + \varphi_0\right]$ denote the azimuthal angles of the m-th receiving antenna and the n-th transmitting antenna respectively, and R_{t} and R_{r} are the radii of the transmit UCAs and the receive UCAs, respectively. We denote by $h_s(d_{mn}^{\mathrm{d}})$ and $h_s(d_{mn}^{\mathrm{r}}) \cdot e^{-j2\pi s\tau_{mn}/Sf_s}$ the channel amplitude gains of direct link and the reflected link corresponding to the s-th subcarrier, respectively. Hence, the channel matrices can be expressed as $\mathbf{H}_{\mathrm{d}} = [h_s(d_{mn}^{\mathrm{d}})]_{M\times N\times S}$ and $\mathbf{H}_{\mathrm{r}} = [h_s(d_{mn}^{\mathrm{r}}) \cdot e^{-j2\pi s\tau_{mn}/Sf_s}]_{M\times N\times S}$ respectively, where τ_{mn} is the time delay between the direct and reflected path expressed as $(d_{mn}^{\mathrm{r}} - d_{mn}^{\mathrm{d}})/c$.

Thereby, at receiver end we can derive the received signal, denoted by $y_{s,m}(t)$, with respect to the s-th subcarrier for the m-th ($0 \le m \le M-1$) receive array element as

$$\begin{aligned} y_{s,m}(t) = &\sum_{n=1}^{N} h_s(d_{mn}^{\mathrm{d}})\delta(t) \otimes x_{s,n}^{\mathrm{d}}(t) \\ &+ \sum_{n=1}^{N} h_s(d_{mn}^{\mathrm{r}}) \cdot e^{-j2\pi\tau_{mn}\frac{s}{S}f_s}\delta(t-\tau_{mn}) \otimes x_{s,n}^{\mathrm{r}}(t) \\ &+ n_{s,m}(t) \end{aligned} \quad (7)$$

where $n_{s,m}(t)$ is the received additive white Gaussian noise (AWGN) corresponding to the s-th subcarrier on the m-th receive array-element, and $\otimes$ represents the convolution operation.

We sample the received signal $y(t)$ by performing an S-point IDFT in frequency domain at the interval of $t = kT_s/S$ ($0 \le k \le S-1$), in which T_{s} denotes the transmit OFDM-OAM duration. And then, the matrix form of the received vortex signal in OFDM-OAM system becomes

$$\begin{aligned} \mathbf{y} &= \mathbf{H}_{\mathrm{d}}\mathbf{X}_{\mathrm{d}} + \mathbf{H}_{\mathrm{r}}\mathbf{X}_{\mathrm{r}} + \mathbf{n} \\ &= \mathbf{H}_{\mathrm{d}}\mathbf{G}(\mathbf{P}\mathbf{s}\mathbf{F}_{\mathrm{S}}^{\mathrm{H}}) + \mathbf{H}_{\mathrm{r}}\bar{\mathbf{G}}(\mathbf{P}\mathbf{s}\mathbf{F}_{\mathrm{S}}^{\mathrm{H}}) + \mathbf{n} \end{aligned} \quad (8)$$

where $\mathbf{s} = [s(0), s(1), \cdots, s(s), \cdots, s(S-1)]$ is the $L \times S$ OFDM information symbol blocks, $\mathbf{P} \in \mathbb{C}^{L\times S}$ is the power allocation matrix with entry $p_{l,s}$ for the (l, s)-th OFDM-OAM subchannel, $\mathbf{F}_S^{\mathrm{H}} \in \mathbb{C}^{L\times S}$ is S-point IDFT OFDM modulation matrix in frequency domain corresponding to the whole OAM-modes, $\mathbf{G} = [\mathbf{g}_0, \mathbf{g}_1, \ldots, \mathbf{g}_l, \ldots, \mathbf{g}_{L-1}]_{N\times L}$ is OAM modulation generation matrix for the transmitting UCAs in which the feed vector with an OAM mode of l is $\mathbf{g}_l = 1/\sqrt{N} \cdot [1, e^{jl2\pi/N}, \cdots, e^{jl2\pi(N-1)/N}]^T$, and $\bar{\mathbf{G}}$ denotes the conjugate of matrix $\mathbf{G}$; $\mathbf{n} = [n_1(t), n_2(t), \ldots, n_m(t), \ldots, n_M(t)]^{\mathrm{T}}$ is the vector of the received noise, in which n_m(t) is additive white Gaussian noise (AWGN) with variance σ_m^2 for the m-th receive array-element. In this paper, we assume that the variances of the received noise for all subcarriers are the same. Note that $[\cdot]^{\mathrm{T}}$ and $[\cdot]^{\mathrm{H}}$ represent the transpose and the conjugate transpose operation, respectively.

The each group of the OFDM information symbols block in Eq. (3) and (4) can be recovered by performing an M-point discrete Fourier transform (DFT) for OAM mode demodulation. Thus, we can get

$$\mathbf{r} = \mathbf{W}\mathbf{y} = \mathbf{W}[(\mathbf{H}_{\mathrm{d}}\mathbf{G} + \mathbf{H}_{\mathrm{r}}\bar{\mathbf{G}}) \cdot (\mathbf{P}\mathbf{s}\mathbf{F}_S^{\mathrm{H}}) + \mathbf{n}] \quad (9)$$

where $\mathbf{H}_{\mathrm{OAM}} = \mathbf{W} \cdot (\mathbf{H}_{\mathrm{d}}\mathbf{G} + \mathbf{H}_{\mathrm{r}}\bar{\mathbf{G}})$ is the OAM channel, $\mathbf{W} = [\mathbf{w}_0, \mathbf{w}_2, \ldots, \mathbf{w}_l, \ldots, \mathbf{w}_{L-1}]^{\mathrm{T}}$ is the $L\times M$ OAM demodulation matrix in which the vector of the single-mode OAM of l is $\mathbf{w}_l = \frac{1}{\sqrt{M}}[1, e^{-jl2\pi/M}, \cdots, e^{-jl2\pi(M-1)/M}]$.

The original emitted signals can be recovered by performing an additional S-point DFT for OFDM demodulation. Thus, the $M\times 1$ demodulated OFDM-OAM signal vector corresponding to the s-th OFDM subcarrier is given by

$$\mathbf{r}(s) = \mathbf{H}_{\text{OFDM-OAM}}^{s}\mathbf{s}(s) + \tilde{\boldsymbol{n}}(s) \quad (10)$$

where $\mathbf{H}_{\text{OFDM-OAM}}^{s} = \mathbf{W} \cdot (\mathbf{H}_{\mathrm{d}}(s)\mathbf{G} + \mathbf{H}_{\mathrm{r}}(s)\bar{\mathbf{G}})$ denotes the OFDM-OAM subchannel for the s-th subcarrier. Since $\mathbf{F}_S$ and $\mathbf{W}$ cannot change the noise energy, $\tilde{\boldsymbol{n}}(s) = \mathbf{W}\mathbf{n}\mathbf{F}_s$ have the same distribution with $n(s)$.

Under the assumption that inter-mode and inter-symbol interference is ignored, the total capacity of the OFDM-OAM communications, denoted by $C_{\mathrm{OFDM-OAM}}$, using the conventional water-falling power allocation algorithm in two-path channel can be derived as follows

$$C_{\text{OFDM-OAM}} = \sum_{s=0}^{S-1}\sum_{l=\lfloor -N/2+1\rfloor}^{\lfloor N/2\rfloor} \log_2(1 + \frac{p_{l,s}h_{l,s}^2}{\sigma_{l,s}^2}) \quad (11)$$

where $h_{l,s}^2$, $\sigma_{l,s}^2$ and $p_{l,s}$ denote the channel amplitude gain, received noise variance and transmit power with respect to the (l, s)-th OFDM-OAM subchannel respectively, $\gamma_{l,s} = h_{l,s}^2/\sigma_{l,s}^2$ represents the received signal-to-noise ratio (SNR) corresponding to the (l, s)-th subchannel, and the power factor $p_{l,s}$ satisfies $\sum_{s=0}^{S-1}\sum_{l=\lfloor -N/2+1\rfloor}^{\lfloor N/2\rfloor} p_{l,s} = P_T$ according to the principle of the traditional water-filling algorithm.

Consider the OFDM-OAM system with OAM-modes set $\mathbf{L} = \{0, 2, \ldots, L-1\}$ and subcarriers set $\mathbf{S} = \{0, 2, \ldots, S-1\}$, the total number of subchannels is $L \times S$. Figure 2 gives an example of channel qualities of the presented OFDM-OAM communication system for $L = 8$, $S = 8$ and $h = 1.5\lambda$. It can be seen that the channel qualities of subchannels are obviously different, this is because the channel amplitude gains of OFDM-OAM systems both depend on receive aperture and OAM-modes. Notably, the receive aperture of the vortex beams with low order OAM-modes might smaller than that with high order OAM-modes. Meanwhile, the reflect ray might enhance the receiving power

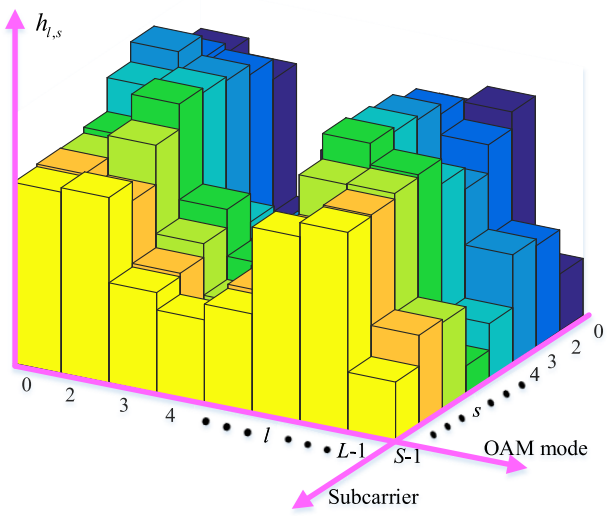

FIGURE 2. Channel qualities of the OFDM-OAM communications.

Step 2 MSPA method for inner-layer optimization

Input: $\mathbf{R} = \{\gamma_{l,s} | l \in \mathbf{M}\}, \mathbf{M} = \{l | l \in \mathbf{L}\}, P_{\mathrm{T}}$

Output: $\mathbf{P} = \{p_l | l \in \mathbf{M}\}$

1: Sort $\mathbf{R}$ in a descending order to $\mathbf{R}'$
2: Compute $\mathbf{P}$ with Eq. (13) for $\forall \gamma_{l,s} \in \mathbf{R}'$
3: **while** p_L<0 **do**
4: Set $L \rightarrow i$, 0 $\rightarrow$temp
5: **for** $p_i < 0$ **do**
6: temp $\leftarrow p_i$+temp
7: $p_i \leftarrow 0$
8: $i \leftarrow i$-1
8: **end for**
9: ε = temp/i
10: $p_i = p_i + \varepsilon$
11: $L \leftarrow i$
12: **end while**

FIGURE 3. Inner-layer optimization problem for OAM modes.

when the LoS and reflection signals are in phase. Thereby, with the order of OAM-mode increasing, the channel amplitude gains of OFDM-OAM communications does not necessarily decrease. Hence, the result proves that the common equal power allocation (EPA), the fixed system power allocation algorithms and are not optimal algorithms to maximize the channel capacity with low complexity for OFDM-OAM communications. Thereby, it is still challenging to investigate an optimal power allocation algorithm with relatively low complexity for achieving the goal of the maximum capacity for OFDM-OAM communications in multipath environments.

III. THE PROPOSED POWER ALLOCATION ALGORITHM

In the section, we propose an efficient power allocation algorithm based on the water-filling allocation scheme that is expected to maximize the channel capacity for OFDM-OAM communications with relatively low computational complexity under the constraint of total transmit power. In this paper, regarding the power $p_{l,s}$ in each subchannel as constants, and $\mathbf{P} = \{p_{l,s} | l \in \mathbf{L}, s \in \mathbf{S}\}$, the power allocation method can be obtained by solving the follow optimization problem,

$$\max C_{\text{OFDM-OAM}} = \sum_{s=0}^{S-1} \sum_{l=\lfloor -N/2+1 \rfloor}^{\lfloor N/2 \rfloor} \log_2(1 + \frac{p_{l,s} h_{l,s}^2}{\sigma_{l,s}^2})$$
$$s.t. \sum_{s=0}^{S-1} \sum_{l=\lfloor -N/2+1 \rfloor}^{\lfloor N/2 \rfloor} p_{l,s} \leq P_T$$
$$p_{l,s} \geq 0, \quad \forall l \in L, \ \forall s \in S \tag{12}$$

The maximum channel capacity problem in Eq. (12) is a strictly convex optimization problem. To control the transmit power of OAM-modes flexibility and ensure the maximum of channel capacity with relatively low complexity, a robust optimal power allocation (ROPA) algorithm combining the mode selected power allocation (MSPA) method and the binary search power allocation (BSPA) method is proposed. Inspired by literature [26], we divide the whole optimization, indicated by (12), into a two-layer optimization problem: the inner-layer is the power allocation for the OAM-modes set L, and the outer-layer is the power allocation for OFDM subcarrier set S.

First, we regard the channel quality of OAM modes as constants and implement the inner-layer optimization problem based on MSPA method. Similar to the linear water-filling method, the MSPA method continuously modifies the allocated powers for each subchannel. In particular, the MSPA method effectively utilizes the channel qualities of various OAM-modes to realize the goal of the maximum capacity quickly. Afterwards, the outer-layer optimization problem can be solved by adopting the BSPA method, which has the advantage of relatively stable iteration numbers with the increasing of the number of OFDM subcarriers.

The detailed processes of proposed algorithm are as follows.

Step 1: initialization. We represent the sets of OAM-modes and subcarriers as $\mathbf{L}$ and $\mathbf{S}$, respectively. The total transmit power is denoted as P_{T}. Initializing SNR by $\{\gamma_{l,s} | l \in \mathbf{L}, s \in \mathbf{S}\}$.

Step 2: inner-layer optimization problem. Figure 3 shows the optimal problem for OAM-modes on the s-th OFDM subcarrier based on MSPA method. We firstly search the maximum SNR for all OAM-modes on the s-th subcarrier, denoted by $\mathbf{R} = \{\gamma_{l,m} \geq \gamma_{l,s}, \forall l \in L, \forall m, s \in \mathbf{S}\}$. Without loss of generality, we sort $\mathbf{R}$ in a descending order in terms of the channel qualities of different OAM-modes. Then the allocated power to the l-th OAM-mode is calculated by

$$p_l = \left(P_{\mathrm{T}} + \sum_{l=\lfloor -N/2+1 \rfloor}^{\lfloor N/2 \rfloor} \frac{1}{\gamma_{l,s}} \right) / L - \frac{1}{\gamma_{l,s}}, \quad \forall l \in \mathbf{R}' \tag{13}$$

Step 3 BSPA method for outer-layer optimization

Input: $\mathbf{Y} = \{\gamma_{k,s} | k \in \mathbf{K}\}, \mathbf{P} = \{p_k | k \in \mathbf{K}\}$

Output: $\mathbf{P}'' = \{p_k | k \in \mathbf{K}\}$

1: **initialize**: Set $a = \min(\gamma_{k,s}), \forall k \in \mathbf{K}$,
$b = \max(\gamma_{k,s}), \forall k \in \mathbf{K}, \Delta$
2: Let $u = (a+b)/2$
3: Calculate $\mathbf{P}'$ with Eq. (14)
4: **while** $\text{abs}(\sum_{s\in\mathbf{S}} p_{k,s} - p_k) > \Delta$ **do**
5: Calculate $\mathbf{P}''$ with Eq. (13)
6: **if** $\sum_{s\in\mathbf{S}} p_{k,s} - p_s > \Delta$ then
7: $u \to a$
8: **else** $u \to b$
9: **end if**
10: Update u
11: **end while**

FIGURE 4. Outer-layer optimization problem for subcarriers.

The allocated transmit power corresponding to the OAM-modes is also decreasingly ordered as $\gamma_{l,s}$ decreases. Afterwards, if $P_L < 0$, the negative transmit powers will be averaged over other subchannels applying cross-zero adjustment [27], and set to zero. The same process is performed until the power over the OAM subchannels is positive, which means acquiring the optimal allocated power to all the OAM modes.

Step 3: outer-layer optimization problem. The optimal process is described in Figure 4. The set of transmit modes $\mathbf{K}$ is firstly obtained by retaining the OAM-modes with positive allocated power in $\mathbf{M}$, and recorded as $\mathbf{K} = \{k \,|p_k > 0 \& k \neq \pm l, \forall k, l \in \mathbf{M}\}$. And then we initialize the upper and lower bounds of the binary search algorithm using the minimum SNR and the maximum SNR of each OAM-modes, denoted by $\min(\gamma_{k,s}), \forall k \in K$ and $\max(\gamma_{k,s}), \forall k \in \mathbf{K}$, respectively. Further, the water-filling level u can be expressed as $(a+b)/2$.

According to (12), the optimal solution can be calculated as follows

$$p_{k,s} = \left[\frac{1}{u} - \frac{1}{\gamma_{k,s}}\right]^+, \quad \forall k \in \mathbf{K} \tag{14}$$

where $[\cdot]^+ = \max(\cdot, 0)$.

The key challenges of the outer-layer optimization problem in essence is to search a proper water-filling level u at each iteration in order to obtain the optimal solution for $\forall s \in S$. For a given positive Δ, the water-falling level u is used to update the lower-bound a if $\sum_{s\in S} p_{k,s} - p_k > \Delta$ for the current k. On the contrary, the upper-bound b is updated as $b = u$. The allocated powers of all the subcarriers for the current OAM mode can be obtained when the optimal solution converges, i.e. $\text{abs}(\sum_{s\in S} p_{k,s} - p_k) < \Delta$.

Compared with the whole optimal problem indicated by Eq. (12), because positive and negative OAM-modes have the same transmission performance, the proposed algorithm can effectively control channel performance of the transmission OAM modes and achieve optimal power allocation to maximize capacity of the OFDM-OAM systems.

Clearly, we find that the complexity of MSPA method varies linearly with the number of OAM-modes. Instead, by adjusting the water-filling level iteratively in the BSPA method, MSPA method allocates the transmit power over each subchannel by utilizing OAM mode differences based on linear iteration method. The BSPA and linear iteration method require the operations of $O[\kappa \times (3L+1) + 2L + 2]$ and $O[\delta \times (L+2) + L \times \log_2 L + 2L + 3]$. Note that the MSPA method does not require exhaustive sorting of the channel power gains, and thus the method requires the operations of $O[\hbar \times (L+1) + 2L + 2]$ only, where κ, $\hbar$ and δ denote the required number of iterations for three methods respectively while satisfying the constraints $\kappa > \hbar \approx \delta$. Consequently, the proposed MSPA's computational complexity is relatively low, especially for the OAM modes of 6∼9, so that the combination of the proposed and BSPA methods can be applied to the wireless OFDM-OAM systems.

IV. RESULTS AND DISCUSSIONS

In this section, simulations are carried out to quantitatively analyze the performance of the proposed power allocation algorithm for the OFDM-OAM system under two-path propagation conditions. The goal of this paper is to analyze how to achieve OFDM-OAM system power allocation with relatively low complexity under different system parameters, therefore we ignore the inter-mode and inter-symbol interference.

The default simulation parameters are configured as follows: the first subcarrier frequency f_0 is 3 GHz, the wavelength λ is 0.1 m, the interval of OFDM subcarriers is 60 kHz, the number of transmitting and receiving elements and the degrees of freedom of multiplexing and demultiplexing satisfy $L = N = M$, the radii of the transmit and receive UCAs are both set to λ, and the transmission distance D is set as 4λ.

Figure 5 depicts our developed ROPA algorithm for the power allocations of multi-mode OFDM-OAM system in two-path channel environment with different reflector distances, where the number of OAM modes and OFDM subcarriers is both set by 16. We also set $h = 0.5\ \lambda$ and λ respectively. As shown in Fig. 5, unlike BSPA algorithm that almost allocate power to different OAM modes averagely, the proposed ROPA algorithm only allocates power to the low order OAM-modes based on channel quality, which is consistent with the wavefront phase property of OAM waves. There is little power allocated to the high order of OAM-modes. The lower the order of OAM-mode, the more OFDM subcarriers that can be allocated to part of the power, which is beneficial

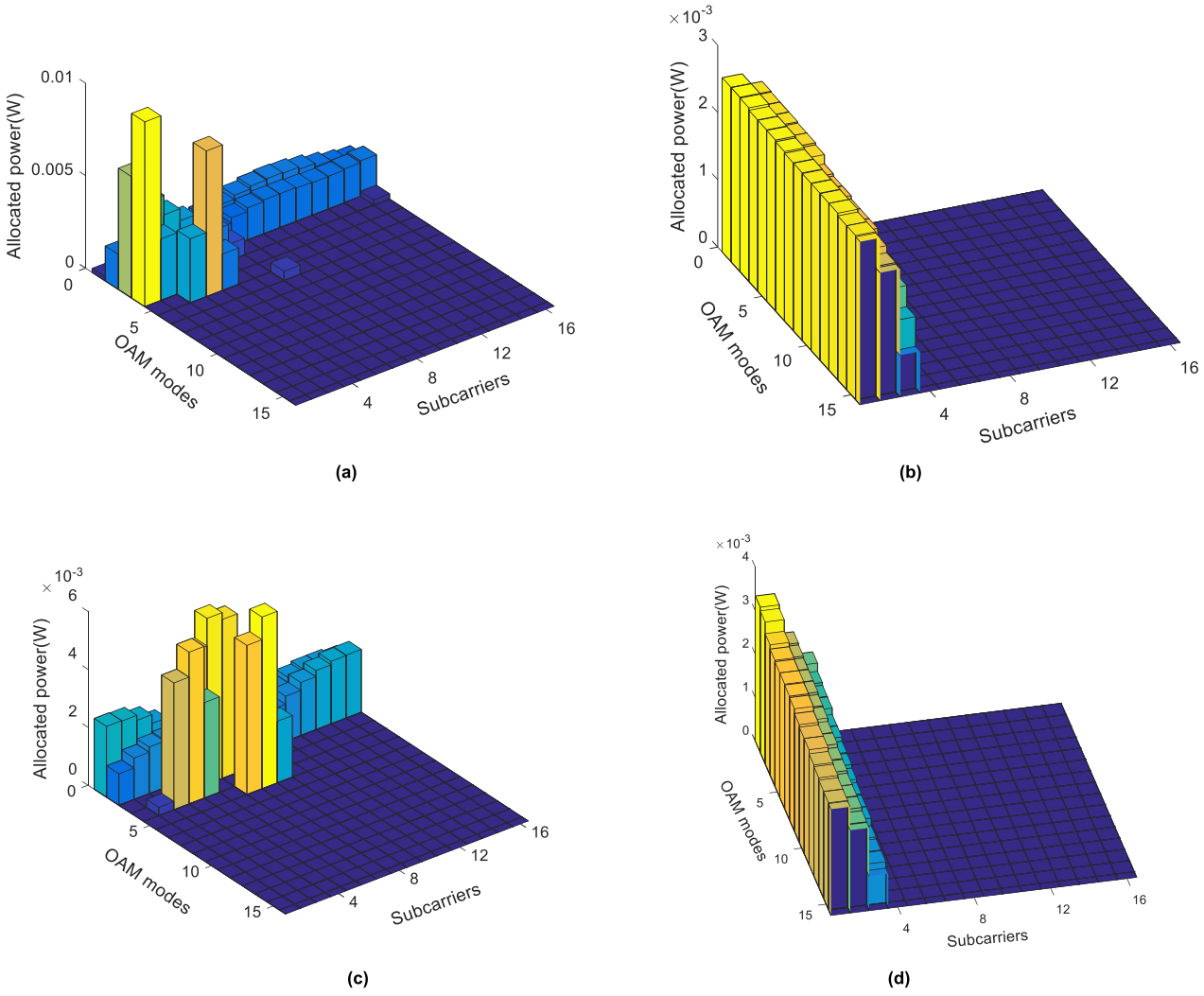

FIGURE 5. Power allocations for OFDM-OAM communications with L = 16 and S = 16 in two-path propagation channel. (a) ROPA, h= λ. (b) BSPA, h= λ. (c) ROPA, h = 0.5 λ. (d) BSPA, h = 0.5 λ.

to reduce multipath-induced intra-channel and inter-channel crosstalk between OAM modes using effective OFDM subcarriers. Fig. 5 (a) and (c) respectively describe the power allocations of ROPA algorithms for $h = \lambda$ and 0.5 λ. We can observe that the closer the reflector, the more the subcarriers allocated power over low order OAM-modes, the larger is the fluctuation in power. This is because the received power from the reflection path increase with the decrease of reflector distance, and the total collected power from the reflected path also increases significantly due to the divergence of OAM beams.

Figure 6 depicts the allocated power versus OAM modes of OFDM-OAM communications under various channel conditions. We set SNR = 30 dB, $L = 8$, $h = \lambda$ for the LoS and the two-path channel conditions, and also set the different reflector distances ($h = 0.5\ \lambda, \lambda, 1.5\ \lambda$) for $L = 16$ in the two-path channel. As shown in Fig. 6, the following two results are observed. First, the allocated power will not change with OAM modes for BSPA algorithm for the cases of $L = 16$ in LoS and two-path channel environments. Second, the number of OAM modes assigned power is more than that of the LoS transmission at the condition of two-path transmission. This is because inner-layer optimization problem effectively utilizes the channel quality of OAM modes. The allocated power for $L = 8$ is larger than that for $L = 16$ with different values of l ranging from 1 to 3. Meanwhile, as we expected the power allocation of OFDM-OAM system in two-path channel decrease as the value of OAM mode increases until reaching to zero. Although there is 75% power allocated to the low order OAM-modes based on the proposed ROPA algorithm for $L = 16$ and $h = \lambda$, the number of OAM modes allocated power increases as the distance of reflector increase. This indicates that there is more high order OAM-modes used to multiplex information in multipath channel to achieve the improvement of system capacity for OAM communications.

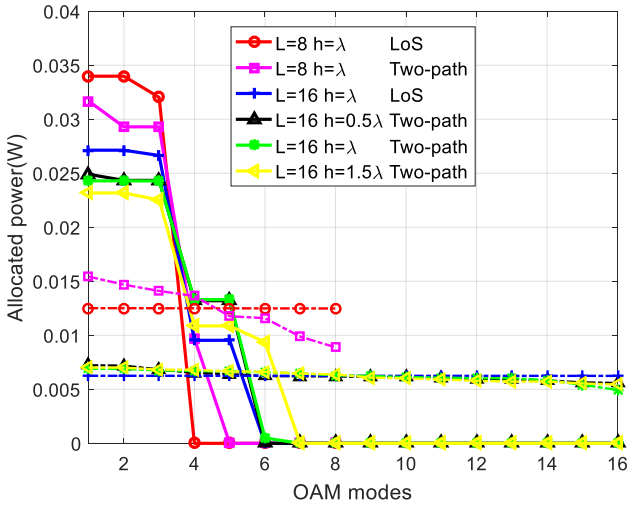

FIGURE 6. Allocated power versus OAM modes for various reflection distances under two channel conditions. Solid lines are MSPA algorithm, and the dashed lines are BPSA algorithm.

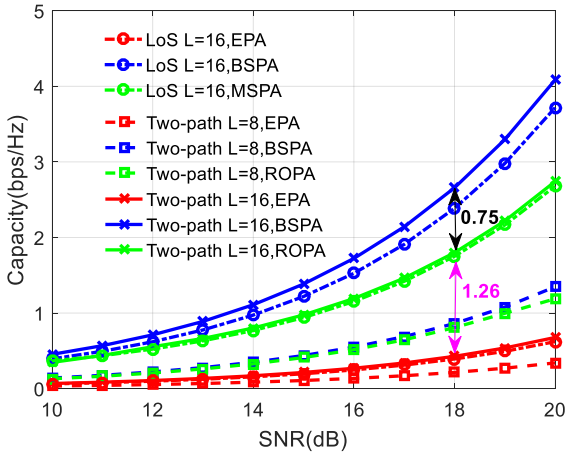

FIGURE 7. Capacity versus SNR with different power allocation algorithms and OAM modes for two propagation conditions.

To evaluate the performance of the proposed algorithm for OFDM-OAM communications in multipath environments, Figure 7 reveals the channel capacity versus SNR with different OAM modes and power allocation algorithms, where the reflector distance and the number of OFDM subcarriers are set as λ and 64, respectively. It can be observed from Fig.7 that the channel capacity in two-path propagation scenarios is consistent with the LoS scenario, it is reasonable because even though the reflected paths are likely to distort the intensity profile and the spiral wavefront of the received signals, powers allocated to the positive and negative modes are nearly the same. Clearly, with SNR increasing, the channel capacities of three allocation schemes increase gradually, which is consistent with this prediction. Although the capacity of ROPA is lower than BSPA, it's obvious that the capacity of ROPA is higher than common EPA. More importantly, the ROPA algorithm achieves a capacity gain of 1.26 bps/Hz at a receiver SNR of 18 dB compared with the EPA method.

Combined with the results shown in Fig. 5, we can conclude that the capacity gains can be achieved when the

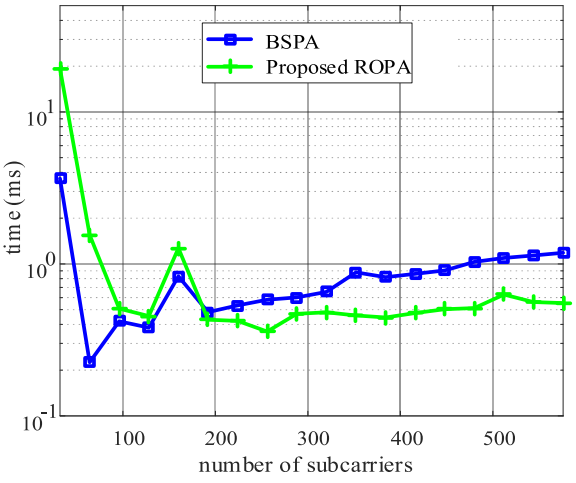

FIGURE 8. Comparison of processing time of the two algorithms.

OFDM-OAM system multiplexes more OAM-modes without an additional frequency band in two-path transmission case. As for example, the capacity gains of BSPA and ROPA algorithms are approximate 2.8 and 2.3 times for SNR = 20 dB, respectively.

Although the channel performance of the proposed ROPA algorithm is lower than that of BSPA algorithm for SNR<20dB, but better than EPA algorithm, the channel quality of OAM mode is used to reduce the number of iterations and shorten the running time, especially when the number of subcarriers is large enough. Figure 8 compares the processing time of the proposed ROPA and BSPA algorithms, where L and SNR are set to 16 and 30 dB respectively. It is seen that the proposed ROPA algorithm has lower processing time than the BSPA algorithm when the number of subcarriers is more than 200. This is because the proposed ROPA algorithm removes the water-filling level searching in power allocation of OAM modes by taking advantage of the channel qualities of OAM subchannels. Hence, we consider the proposed ROPA algorithm as an optimal scheme with good performance and relatively low time complexity.

V. CONCLUSION

In summary, we investigated the power allocation for multi-mode OFDM-OAM communications under two-path transmission conditions. The OFDM-OAM communication system model with multiple OAM-modes multiplexing is first build up on the basis of an ideal reflector, and then channel capacity is derived detailly. Moreover, an robust optimal power allocation algorithm considering OAM-modes and OFDM subcarriers constraints is then proposed for capacity maximization under various multipath propagation conditions by taking advantage of the channel quality of OAM subchannels to remove the water-filling level searching. The results of our investigation focus on the fundamental effect of two-path channel on allocation performance by considering different OAM modes, different reflector distances and SNR. The simulation results show that the proposed algorithm

can allocate power to almost all subcarrier of low order OAM- modes and achieves a considerable capacity gains compared with the EPA algorithm for two-path channels. Further work may extend the algorithm to six-path or ten-path channel for OFDM-OAM communications. Besides, the optimal power allocation algorithm for OAM-MIMO communication, inter-mode interference mitigation, and OAM beam convergence are also important direction for our future work.

REFERENCES

[1] L. Allen, M. W. Beijersbergen, R. J. C. Spreeuw, and J. P. Woerdman, "Orbital angular momentum of light and the transformation of Laguerre–Gaussian laser modes," *Phys. Rev. A, Gen. Phys.*, vol. 45, no. 11, pp. 8185–8189, Jun. 1992.

[2] B. Thidé, H. Then, J. Sjöholm, K. Palmer, J. Bergman, T. D. Carozzi, Y. N. Istomin, N. H. Ibragimov, and R. Khamitova, "Utilization of photon orbital angular momentum in the low-frequency radio domain," *Phys. Rev. Lett.*, vol. 99, no. 8, Aug. 2007, Art. no. 087701.

[3] S. Mohaghegh Mohammadi, L. K. S. Daldorff, J. E. S. Bergman, R. L. Karlsson, B. Thide, K. Forozesh, T. D. Carozzi, and B. Isham, "Orbital angular momentum in Radio—A system study," *IEEE Trans. Antennas Propag.*, vol. 58, no. 2, pp. 565–572, Feb. 2010.

[4] R. Chen, H. Zhou, M. Moretti, X. Wang, and J. Li, "Orbital angular momentum waves: Generation, detection and emerging applications," *IEEE Commun. Surveys Tuts.*, vol. 22, no. 2, pp. 840–868, 2nd Quart., 2020.

[5] V. W. S. Wong, *Key Technologies for 5G Wireless Systems*. Cambridge, U.K.: Cambridge Univ. Press, 2017.

[6] A. E. Willner, Y. Ren, G. Xie, Y. Yan, L. Li, Z. Zhao, J. Wang, M. Tur, A. F. Molisch, and S. Ashrafi, "Recent advances in high-capacity free-space optical and radio-frequency communications using orbital angular momentum multiplexing," *Phil. Trans. Roy. Soc. A, Math., Phys. Eng. Sci.*, vol. 375, no. 2087, Feb. 2017, Art. no. 20150439.

[7] L. Wang, X. Ge, R. Zi, and C.-X. Wang, "Capacity analysis of orbital angular momentum wireless channels," *IEEE Access*, vol. 5, pp. 23069–23077, 2017.

[8] A. Trichili, K.-H. Park, M. Zghal, B. S. Ooi, and M.-S. Alouini, "Communicating using spatial mode multiplexing: Potentials, challenges, and perspectives," *IEEE Commun. Surveys Tuts.*, vol. 21, no. 4, pp. 3175–3203, May 2019.

[9] Z. Wei, L. Yang, D. W. K. Ng, J. Yuan, and L. Hanzo, "On the performance gain of NOMA over OMA in uplink communication systems," *IEEE Trans. Commun.*, vol. 68, no. 1, pp. 536–568, Jan. 2020.

[10] Z. Zhang, S. Zheng, Y. Chen, X. Jin, H. Chi, and X. Zhang, "The capacity gain of orbital angular momentum based multiple-input-multiple-output system," *Sci. Rep.*, vol. 6, no. 1, p. 25418, May 2016.

[11] K. A. Opare, Y. Kuang, and J. J. Kponyo, "Mode combination in an ideal wireless OAM-MIMO multiplexing system," *IEEE Wireless Commun. Lett.*, vol. 4, no. 4, pp. 449–452, Aug. 2015.

[12] R. Gaffoglio, A. Cagliero, A. D. Vita, and B. Sacco, "OAM multiple transmission using uniform circular arrays: Numerical modeling and experimental verification with two digital television signals," *Radio Sci.*, vol. 51, no. 6, pp. 645–658, Jun. 2016.

[13] R. Chen, H. Xu, M. Moretti, and J. Li, "Beam steering for the misalignment in UCA-based OAM communication systems," *IEEE Wireless Commun. Lett.*, vol. 7, no. 4, pp. 582–585, Aug. 2018.

[14] K. Zhang, Y. Wang, Y. Yuan, and S. N. Burokur, "A review of orbital angular momentum vortex beams generation: From traditional methods to metasurfaces," *Appl. Sci.*, vol. 10, no. 3, p. 1015, Feb. 2020.

[15] W. Wei, C. Brousseau, K. Mahdjoubi, and O. Emile, "Generation of OAM waves with circular phase shifter and array of patch antennas," *Electron. Lett.*, vol. 51, no. 6, pp. 442–443, Mar. 2015.

[16] Y. Yan, L. Li, G. Xie, C. Bao, P. Liao, H. Huang, Y. Ren, N. Ahmed, Z. Zhao, Z. Wang, N. Ashrafi, S. Ashrafi, S. Talwar, S. Sajuyigbe, M. Tur, A. F. Molisch, and A. E. Willner, "Multipath effects in millimetre-wave wireless communication using orbital angular momentum multiplexing," *Sci. Rep.*, vol. 6, no. 1, Sep. 2016, Art. no. 33482.

[17] Y. Yao, X. Liang, M. Zhu, W. Zhu, J. Geng, and R. Jin, "Analysis and experiments on reflection and refraction of orbital angular momentum waves," *IEEE Trans. Antennas Propag.*, vol. 67, no. 4, pp. 2085–2094, Apr. 2019.

[18] Y. Yan, L. Li, G. Xie, M. Ziyadi, A. M. Ariaei, Y. Ren, O. Renaudin, Z. Zhao, Z. Wang, C. Liu, S. Sajuyigbe, S. Talwar, S. Ashrafi, A. F. Molisch, and A. E. Willner, "OFDM over mm-Wave OAM channels in a multipath environment with intersymbol interference," in *Proc. IEEE Global Commun. Conf. (GLOBECOM)*, Dec. 2016, pp. 1–6.

[19] R. Chen, W. Yang, H. Xu, and J. Li, "A 2-D FFT-based transceiver architecture for OAM-OFDM systems with UCA antennas," *IEEE Trans. Veh. Technol.*, vol. 67, no. 6, pp. 5481–5485, Jun. 2018.

[20] T. Hu, Y. Wang, X. Liao, J. Zhang, and Q. Song, "OFDM-OAM modulation for future wireless communications," *IEEE Access*, vol. 7, pp. 59114–59125, 2019.

[21] L. Liang, W. Cheng, W. Zhang, and H. Zhang, "Joint OAM multiplexing and OFDM in sparse multipath environments," *IEEE Trans. Veh. Technol.*, vol. 69, no. 4, pp. 3864–3878, Apr. 2020.

[22] K. Son, B. C. Jung, S. Chong, and D. K. Sung, "Power allocation for OFDM-based cognitive radio systems under outage constraints," *Proc. IEEE Int. Conf. Commun. (ICC)*, Cape Town, South Africa, Jul. 2010, pp. 1–5.

[23] J. Jang, K. B. Lee, and Y.-H. Lee, "Transmit power and bit allocations for OFDM systems in a fading channel," in *Proc. IEEE Global Commun. Conf. (GLOBECOM)*, vol. 2, Dec. 2003, pp. 858–862.

[24] D. P. Palomar and J. R. Fonollosa, "Practical algorithms for a family of waterfilling solutions," *IEEE Trans. Signal Process.*, vol. 53, no. 2, pp. 686–695, Feb. 2005.

[25] L. Liang, W. Cheng, W. Zhang, and H. Zhang, "Orthogonal frequency and mode division multiplexing for wireless communications," in *Proc. IEEE Global Commun. Conf. (GLOBECOM)*, Abu Dhabi, United Arab Emirates, Dec. 2018, pp. 1–7.

[26] X. Jiang and C. Zhang, "Secure transmission aided by orbital angular momentum jamming with imperfect CSI," in *Proc. IEEE Int. Conf. Commun. (ICC)*, Shanghai, China, May 2019, pp. 1–6.

[27] X. Ling, B. Wu, P.-H. Ho, F. Luo, and L. Pan, "Fast water-filling for agile power allocation in multi-channel wireless communications," *IEEE Commun. Lett.*, vol. 16, no. 8, pp. 1212–1215, Aug. 2012.

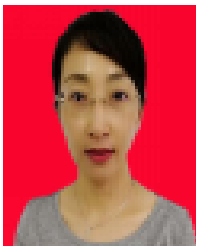

MINGZHE QU received the B.E. and M.S. degrees in electronic engineering from Heilongjiang University, Harbin, China, in 1999 and 2007, respectively. She was with the School of Technology, Harbin University, where she is currently Professor. Her research interests include orbital angular momentum wireless communications and millimeter-wave wireless communications.

YANG WANG (Member, IEEE) received the M.S. and Ph.D. degrees from The University of Sheffield, U.K., in 2011 and 2015, respectively. He joined the School of Communications and Information Engineering, Chongqing University of Posts and Telecommunications (CQUPT), in 2015. He is currently an Associate Professor with the Communication Department, CQUPT. His research interests include antennas and propagation, radar signature management, phase-modulating microwave structures, and wireless communications.

XI LIAO (Member, IEEE) received the B.E. degree in communication engineering from Hohai University, Nanjing, China, in 2011, and the Ph.D. degree in communication and information engineering from Harbin Engineering University, China, in 2015. She was with the Chongqing University of Posts and Telecommunications, in 2016, where she is currently an Associate Professor with the Communication Department. Her main research interests include orbital angular momentum wireless communications, millimeter-wave wireless communications, antennas, and radio propagation.

SHASHA LIAO received the Ph.D. degree in optical engineering from the Huazhong University of Science and Technology, Wuhan, China, in 2017. She is currently a Lecturer with the School of Communication and Information Engineering, Chongqing University of Posts and Telecommunications, China. Her research interests include silicon photonics devices and integrated microwave/millimeter-wave photonics.

JIHUA ZHOU received the Ph.D. degree from the Institute of Computing Technology, Chinese Academy of Sciences, in 2008. He was a Postdoctoral Fellow with Tsinghua University, in 2012. He has been a Researcher and held the Chief Engineer of Chongqing Jinmei Communication Company Ltd. His current research interests include wireless communication, mobile networks, and intelligent cluster.